Theor Chem Acc (2007) 117: 275–281
DOI 10.1007/s00214-006-0136-y

REGULAR ARTICLE

**Shuqiang Niu · Toshiko Ichiye**

# Probing the structural effects on the intrinsic electronic and redox properties of [2Fe–2S]$^{+}$ clusters, a broken-symmetry density functional theory study

Received: 30 June 2005 / Accepted: 2 December 2005 / Published online: 13 July 2006


**Abstract** In biological electron transport chains, [2Fe–2S] clusters have versatile electrochemical properties and serve as important electron carriers in a wide variety of biological processes. To understand structural effects on the variation in reduction potentials in [2Fe–2S] proteins, a series of [2Fe–2S] protein analogs with bidentate ligands ($-SC_2H_4NH_2$) were recently produced by collision-induced dissociation of $[Fe_4S_4(L)_4]^{2-}$($L = SC_2H_4NH_2$). Combined with photoelectron spectroscopy findings, the reaction mechanisms of $[Fe_4S_4(L)_4]^{2-}$ to $[Fe_2S_2(L)_2]^{-}$ and the structural effects of ligands on the electronic and redox properties of the [2Fe–2S] clusters are investigated here using broken-symmetry density functional theory method. Our calculations suggest that $[Fe_2S_2(\eta^2-L)(cis-L)]^{-}$ and $[Fe_2S_2(\eta^2-L)_2]^{-}$ are the experimentally observed [2Fe–2S] products, which are generated via a fission process of $[Fe_4S_4(L)_4]^{2-}$ followed by rearrangement of ligands of $[Fe_2S_2(L)_2]^{-}$. Moreover, structural variation of the ferrous center may dramatically affect the oxidation energy of the [2Fe–2S] clusters.

## 1 Introduction

As one of the most ubiquitous and versatile electron carriers, iron–sulfur clusters play an important role in electron transfer of biological systems as well as in biosynthetic and bioregulatory functions [1–5]. The redox sites of iron–sulfur proteins usually contain one, two, three, or four iron atoms tetrahedrally bound by sulfides and cysteine thiolate residues as well as other residues. A variety of studies on different clusters have shown the importance of electrostatic hydrogen bonding and solvent effects. Among these redox agents, the rhombic $Fe_2(\mu_2-S)_2$ core ([2Fe–2S]) demonstrates a multitude of functions. In particular, the [2Fe–2S] clusters have a remarkable facility for conversion into more complex and biological clusters such as [3Fe–4S], [4Fe–4S], and [8Fe–8S] clusters [1,6]. In biological electron transport chains, the [2Fe–2S] units have versatile electrochemical properties with reduction potentials ranging from −450 to −150 mV versus NHE for the $[Fe_2S_2]^{2+/1+}$ redox couple for standard ferredoxins [7] (Scheme 1), serving as important electron carriers in a wide variety of biological processes. The Reiske-type proteins contain a variant cluster, in which two of the ligating cysteines are replaced by histidines, and have reduction potentials from about −100 to +400 mV [8]. Although various experimental [8–10] and computational techniques [11–13] have been concerned with the pH dependence of reduction potentials of these iron–sulfur clusters, the influence of intrinsic factors on the reduction potentials of the [2Fe–2S] clusters is not fully understood.

A symmetric fission process of doubly charged [4Fe–4S] cubane anions into two identical singly charged [2Fe–2S] clusters with both iron sites tri-coordinated was discovered previously [14]. Our previous density functional theory (DFT) studies of the disassembly mechanism of $[Fe_4S_4Cl_4]^{2-}$ to $[Fe_2S_2Cl_2]^{-}$ suggested that the produced [2Fe–2S] clusters are low-spin state with $S = 1/2$, which is the lowest energy state of the [2Fe–2S] clusters [15]. More recently, the fission of the precursor cubane complexes $[Fe_4S_4(SEt)_{4-n}L_n]^{2-}$($n = 0-4$) into the products, $[Fe_2S_2(SEt)_{2-m}L_m]^{-}$($L = -SC_2H_4NH_2$, $m = 0-2$), have been observed by CID and photoelectron spectroscopy experiments [16]. Interestingly, an additional feature was observed in the spectra of $[Fe_2S_2L_2]^{-}$, indicating the formation of

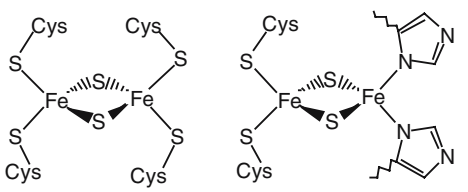


standard ferredoxin  Rieske-type protein

**Scheme 1**

S. Niu · T. Ichiye (✉)
Department of Chemistry, Georgetown University,
Washington, DC 20057-1227, USA
E-mail: ti9@georgetown.edu

a new isomer with a decrease of 0.55 eV in the oxidation energy. Although the preliminary DFT calculations suggested that bidentate coordination of the [2Fe–2S] cluster in which the $NH_2$ group also coordinates the iron might result in significant variations in the oxidation energies, it is necessary to completely understand how the bidentate ligands stabilize the [2Fe–2S] cluster and affect the electronic and redox properties of the [2Fe–2S] clusters.

Here we report a detailed broken-symmetry (BS) DFT study of the structural, electronic, and redox properties of various possible coordination geometries produced by CID of [4Fe–4S] cubane complexes in the gas phase, including the subsequent ligand rearrangement of the [2Fe–2S] clusters. Combined with available experimental findings in biological and synthetic systems, we found that the structural variation of the ferrous center may dramatically affect the reduction potential of the [2Fe–2S] clusters and that the chelated bidentate ligand on the ferric center significantly stabilizes the clusters.

## 2 Computational details

Since the experimental observations from Mössbauer and EPR spectroscopy suggested that the [2Fe–2S] and [4Fe–4S] clusters are spin-coupled systems [17], the spin polarized or so-called "broken-symmetry" DFT method (BS-DFT) [18, 19] was utilized for geometry optimization and the investigation of the electronic structure of the complexes. Becke's three-parameter hybrid exchange functional [20–22] and the Lee–Yang–Parr correlation functional (B3LYP) [23] with the 6-31G** basis sets [24–26] were used. The calculated energies were refined at the B3LYP/$6-31(++)_S$G**//B3LYP/6-31G** level, where *sp*-type diffuse functions were added to the 6-31G** basis set of the sulfur atoms [24–26]. Transition states (TS) were optimized by an eigenvalue-following optimization method [27,28], in which the final updated Hessian shows only one negative eigenvalue. No symmetry restraints were imposed during geometry optimizations.

Generally, spin-coupled systems are well described by the spin Hamiltonian [29],

$$H_{\text{spin}} = J \sum_{i<j} \hat{S}_i \cdot \hat{S}_j, \tag{1}$$

where $i$ and $j$ represent the high-spin sites and $J$ is the exchange coupling constant. In BS-DFT, the $\alpha$- and $\beta$-spin electrons are treated separately and have different spatial Kohn–Sham (KS) orbitals, which result in different electron density functions $\rho^\alpha$ and $\rho^\beta$. Thus, the additional interactions between the opposite spin electrons in different spatial orbitals can be properly taken into account in the exchange-correlation energy functional. Although the BS-DFT energy of a spin-polarized low-spin state is not a pure spin state energy and instead is a weighted average of pure spin states, it can be corrected by an approximate spin projection procedure based on the method developed by Noodleman [30]. However, since the spin projection corrections for the reduced and oxidized sites of iron–sulfur protein analogs tend to cancel each other in the calculated oxidation energies or relative energies [15,31], the spin projection correction for the BS-DFT energies was neglected in this work.

The intrinsic reduction-free energy ($\Delta G_{\text{int}}$) of the redox site independent of the protein can be regarded as the free energy of an oxidation process of a redox site analog in the absence of solvent and can be obtained by photoelectron spectroscopy measurement [32,33],

$$\Delta G_{\text{int}} = -\text{ADE} = -(\text{VDE} + \lambda_{\text{oxd}}), \tag{2}$$

where the adiabatic detachment energy (ADE) is the energy difference between the reduced and oxidized states, the vertical detachment energy (VDE) is the Frank–Condon energy required to remove an electron, and $\lambda_{\text{oxd}}$ is the oxidant intramolecular relaxation or reorganization energy. Theoretically, these redox properties can be calculated by BS-DFT calculations. Our previous work showed that the B3LYP method gives a reliable description of the structural and redox properties of iron–sulfur clusters with respect to other conventional ab initio and DFT methods [34]. Furthermore, our recent photoelectron spectroscopy and DFT studies on the tetrahedral ferric complexes $Fe^{III}X_4^-$ (X = Cl, Br) and the three-coordinate complexes $M^{II}X_3^-$ (M = Mn, Fe, Co, Ni; X = Cl, Br) have shown that increasing the basis set size for all atoms, for example using triple-$\zeta$ basis sets, does not significantly change the calculated geometric parameters and redox energies with respect to the experimental data or the calculated values using double-$\zeta$ basis sets [35].

All calculations were performed using the NWChem program package [36,37]. The molecular orbital visualizations were performed using the extensible computational chemistry environment (Ecce) application software [38].

## 3 Results and discussion

$[Fe_2S_2(SEt)_{2-m}L_m]^-$(L = $SC_2H_4NH_2$; $m$ = 0, 1, 2) were produced by CID of the $[Fe_4S_4(SEt)_{4-n}L_n]^{2-}$ clusters (L = –$SC_2H_4NH_2$, $n$ = 0–4) [16]. First, the precursor cubane species are discussed, followed by the possible [2Fe–2S] fission species. Finally, the fission and ligand rearrangement mechanisms are investigated to evaluate the experimentally observed products.

### 3.1 Geometries and electronic structure of $[Fe_4S_4(SEt)_{4-n}L_n]^{2-}$(L = –$SC_2H_4NH_2$, $n$ = 0 and 4)

The geometries and electronic structure of $[Fe_4S_4(SEt)_4]^{2-}$ and $[Fe_4S_4L_4]^{2-}$ were investigated and compared to photoelectron spectroscopy study of the precursor cubane complexes $[Fe_4S_4(SEt)_{4-n}L_n]^{2-}$(L = –$SC_2H4NH_2$, $n$ = 1 − 4) [16,32]. Although the various cubane clusters demonstrated very similar spectral patterns, the ADE of $[Fe_4S_4(SEt)_{4-n}L_n]^{2-}$ significantly increases relative to $[Fe_4S_4(SEt)_4]^{2-}$ by 0.13–0.37 eV as $n$ goes from 1 to 4. The structural and energetic properties of $[Fe_4S_4L_4]^{2-}$ have been calculated with different ligand coordination

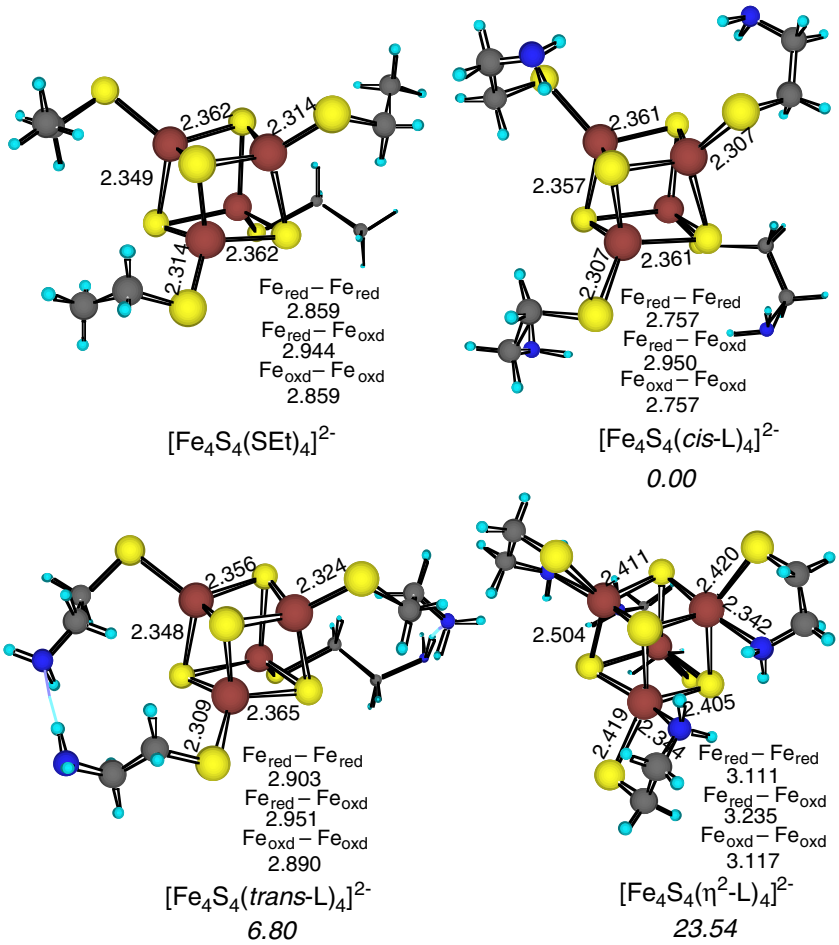


**Fig. 1** The B3LYP/6-31G** optimized geometries and the relative energies (kcal/mol) of $[Fe_4S_4(Set)_{4-n}L_n]^{2-}$ (L = –$SC_2H_4NH_2$, $n$ = 0 and 4). The top layer is the oxidized sublayer of the clusters

patterns since the experimental structure is not known. In $[Fe_4S_4(trans-L)_4]^{2-}$, in which the torsion angle ∠SCCN is 180°, L has a quasi-linear conformation and the $NH_2$ group points away from the cubane core. In $[Fe_4S_4(cis-L)_4]^{2-}$, in which the torsion angle ∠SCCN is −60°, L has a bent conformation and the $NH_2$ group points toward the cubane core. $[Fe_4S_4(\eta^2-L)_4]^{2-}$ can be generated from $[Fe_4S_4(cis-L)_4]^{2-}$ by coordination of the $NH_2$ groups with the iron centers. The B3LYP/6-31G** optimized geometries and the relative energies are shown in Fig. 1. The experimental and calculated ADE and VDE are summarized in Table 1.

In $[Fe_4S_4(trans-L)_4]^{2-}$, there are two intra-molecular hydrogen bonds between the four $NH_2$ groups. The structure of the cluster core is very similar to $[Fe_4S_4(SEt)_4]^{2-}$ except for the Fe–Fe distances on each redox sublayer from 2.86 Å for $[Fe_4S_4(SEt)_4]^{2-}$ to ∼2.90 Å for $[Fe_4S_4(trans-L)_4]^{2-}$. The calculated ADE and VDE of $[Fe_4S_4(trans-L)_4]^{2-}$ increase by 0.16 and 0.13 eV, respectively, relative to those of $[Fe_4S_4(SEt)_4]^{2-}$. Since the oxidation of $[Fe_4S_4(SR)_4]^{2-}$ involves a minority spin electron with the $\sigma_{Fe-Fe}$ bonding and $\sigma^*_{Fe-S}$ antibonding characters [31], the oxidation energy of

**Table 1** Oxidation energies (eV) of $[Fe_4S_4(SEt)_{4-n}L_n]^{2-}$ and $[Fe_2S_2(L)_2]^-$ ($n$ = 0and4; L = –$SC_2H_4NH_2$, SEt = $SC_2H_5$)

| Species[c,d] | ADE[a] | | VDE[b] | |
|---|---|---|---|---|
| | Exp | Cal | Exp | Cal |
| $[Fe_4S_4(SEt)_4]^{2-}$ | 0.29 (6) | 0.19 | 0.52 (6) | 0.48 |
| $[Fe_4S_4(cis-L)_4]^{2-}$ | 0.66 (6) | 0.63 | 0.83 (6) | 0.98 |
| $[Fe_4S_4(trans-L)_4]^{2-}$ | | 0.35 | | 0.61 |
| $[Fe_4S_4(\eta^2-L)_4]^{2-}$ | | −0.74 | | −0.36 |
| $[Fe_2S_2(\eta^2-L)(cis-L)]^-$ | 2.91 (5) | 2.93 | 3.10 (5) | 3.13 |
| $[Fe_2S_2(cis-L)(\eta^2-L)]^-$ | | 2.58 | | 2.79 |
| $[Fe_2S_2(\eta^2-L)_2]^-$ | 2.24 (6) | 2.10 | 2.46 (6) | 2.37 |
| $[Fe_2S_2(cis-L)_2]^-$ | | 3.36 | | 3.58 |

[a] Adiabatic detachment energies. The numbers in the parentheses represent the uncertainties in the last digit

[b] Vertical detachment energies. The numbers in the parentheses represent the uncertainties in the last digit

[c] In $cis-SC_2H_4NH_2$, the torsion angle ∠SCCN is −60°; in $trans-SC_2H_4NH_2$, the torsion angle ∠SCCN is 80°; $\eta^2-L = \eta^2-SC_2H_4NH_2$.

[d] $L_1$ of $[Fe_2S_2(L_1)(L_2)]^-$ is the ligand coordinated to the ferric center in the reduced state, whereas $L_1$ of $[Fe_2S_2(L_1)(L_2)]^-$ is the ligand coordinated to the ferrous center

the cluster should increase with the decrease in the bonding interaction of the terminal Fe–S bonds. Because the donor ability of -$SC_2H_4NH_2$ is only slightly smaller than that of –SEt, the major factor contributing to the changes in the oxidation energy should be the electrostatic effects of the $NH_2$ groups.

In $[Fe_4S_4(cis-L)_4]^{2-}$, the $NH_2$ groups are much closer to the cubane core than those in $[Fe_4S_4(trans-L)_4]^{2-}$. As the positive end of the $NH_2$ dipole points toward the negative core, the oxidized electron of $[Fe_4S_4(cis-L)_4]^{2-}$ is more significantly stabilized relative to $[Fe_4S_4(trans-L)_4]^{2-}$ and $[Fe_4S_4(SEt)_4]^{2-}$, leading to the larger ADE and VDE. The calculated ADE and VDE of $[Fe_4S_4(cis-L)_4]^{2-}$ increase by 0.44 and 0.50 eV, respectively, relative to those of $[Fe_4S_4(SEt)_4]^{2-}$.

Not surprisingly, $\eta^2$-coordination of the bidentate ligands with the iron centers in $[Fe_4S_4(\eta^2-L)_4]^{2-}$ leads to an unstable structure as the irons are five-coordinated. The Fe–S bonds of the redox sublayers of $[Fe_4S4(\eta^2-L)_4]^{2-}$ are significantly increased from 2.36 Å in $[Fe_4S_4(SEt)_4]^{2-}$ to 2.41 Å, while the Fe–Fe distances are significantly increased from 2.86 to 3.11 Å. Upon oxidation of $[Fe_4S_4(\eta^2-L)_4]^{2-}$ to $[Fe_4S_4(\eta^2-L)_4]^{-}$, the chelating interactions of the bidentate ligands with the ferric centers dramatically stabilize the oxidized state, resulting in the negative ADE and VDE of −0.74 and −0.34 eV, respectively.

Overall, the bidentate ligand L prefers a folded *cis*-conformation, $[Fe_4S_4(cis-L)_4]^{2-}$, which is more stable by 6.8 and 23.5 kcal/mol than $[Fe_4S_4(trans-L)_4]^{2-}$ and $[Fe_4S_4(\eta^2-L)_4]^{2-}$, respectively. The calculated ADE and VDE of $[Fe_4S_4(cis-L)_4]^{2-}$ are 0.63 and 0.98 eV, respectively, in very good agreement with the experimental values of 0.66 and 0.83 eV. Thus, we suggest that the ligand in $[Fe_4S_4(SEt)_{4-n}L_n]^{2-}$ acts as a monodentate ligand and that the electrostatic interaction between the polar amino groups and the cubane core plays an important role in the variations in the electron binding energy.

### 3.2 Fission products $[Fe_2S_2(L)_2]^{-}$ (L = –$SC_2H_4NH_2$)

Our previous DFT studies of the disassembly mechanism of $[Fe_4S_4Cl_4]^{2-}$ to $[Fe_2S_2Cl_2]^{-}$ suggested that the fission of the [4Fe–4S] parent can proceed via a spin-localized intermediate to generate the [2Fe–2S] clusters with a low-spin state of $S = 1/2$ [33]. The simplest possible fission species of $[Fe_4S_4(cis-L)_4]^{2-}$ would appear to be $[Fe_2S_2(cis-L)_2]^{-}$ with a low-spin state. However, as the bidentate coordination of the ligand with $Fe^{III}$ may decrease the fission barrier, $[Fe_2S_2(\eta^2-L)(cis-L)]^{-}$, in which the $Fe^{III}$ coordinates with both the sulfur and the $NH_2$ group of the ligand, also appears to be a possible fission species. Our DFT calculations indicate that the fission of $[Fe_4S_4(cis-L)_4]^{2-}$ to $[Fe_2S_2(cis-L)_2]^{-}$ is almost thermo-neutral, similar to the $[Fe_4S_4Cl_4]^{2-}$ results [33], whereas the fission of $[Fe_4S_4(cis-L)_4]^{2-}$ to $[Fe_2S_2(\eta^2-L)(cis-L)]^{-}$ is exothermic by −24.8 kcal/mol (Fig. 2). The corresponding spin-delocalized high-spin species ($S = 9/2$) are less stable by ∼5 kcal/mol

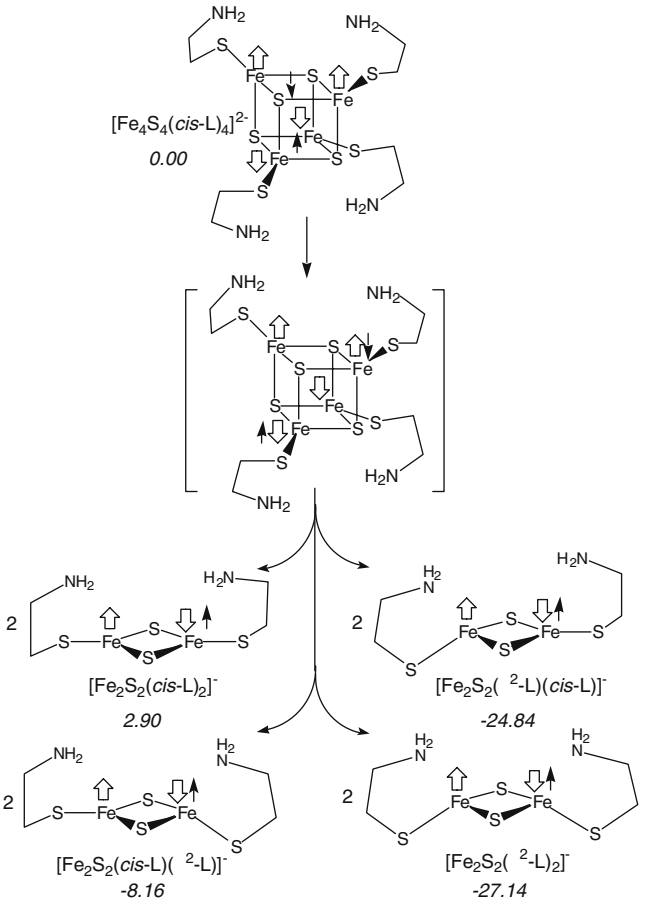


**Fig. 2** Schematic fission reaction pathways and the calculated reaction energies (kcal/mol) of $[Fe_4S_4(cis-L)_4]^{2-}$. The *large hollow arrow* represents the five majority spins, whereas the *small arrow* represents a minority spin on the iron center

than the spin-coupled species ($S = 1/2$). Although two kinds of fission products have also been observed by the photoelectron spectroscopy experiments, the calculated ADE and VDE of $[Fe_2S_2(cis-L)_2]^{-}$ are in disagreement with the experimental values (Table 1). Moreover, the fission of $[Fe_4S_4(cis\,L)_4]^{2-}$ to two other possible products, $[Fe_2S_2(cis-L)(\eta^2-L)]^{-}$ and $[Fe_2S_2(\eta^2-L)_2]^{-}$ (in which the $Fe^{II}$ coordinates with both the sulfur and the $NH_2$ of the ligand), is calculated to be exothermic by −8.16 and −27.15 kcal/mol, respectively, but to $[Fe_2S_2(trans-L)_2]^{-}$ is highly endothermic by 16.5 kcal/mol. Thus, the distinct energy differences between these species imply that $[Fe_2S_2(cis-L)_2]^{-}$ and $[Fe_2S_2(trans-L)_2]^{-}$ are not final fission products in the experiment.

Of the two most stable isomers, the calculated ADE and VDE of $[Fe_2S_2(\eta^2-L)_2]^{-}$ are 2.10 and 2.37 eV, respectively, in very good agreement with the experimental values of 2.24 and 2.46 eV, respectively, and the calculated ADE and VDE of $[Fe_2S_2(\eta^2-L)(cis-L)]^{-}$ are 2.93 and 3.13 eV, respectively, also in very good agreement with the experimental values of 2.91 and 3.10 eV, respectively, (Table 1). Thus, the DFT energy calculations suggest that $[Fe_2S_2(\eta^2-L)(cis-L)]^{-}$ and $[Fe_2S_2(\eta^2-L)_2]^{-}$ are the experimentally

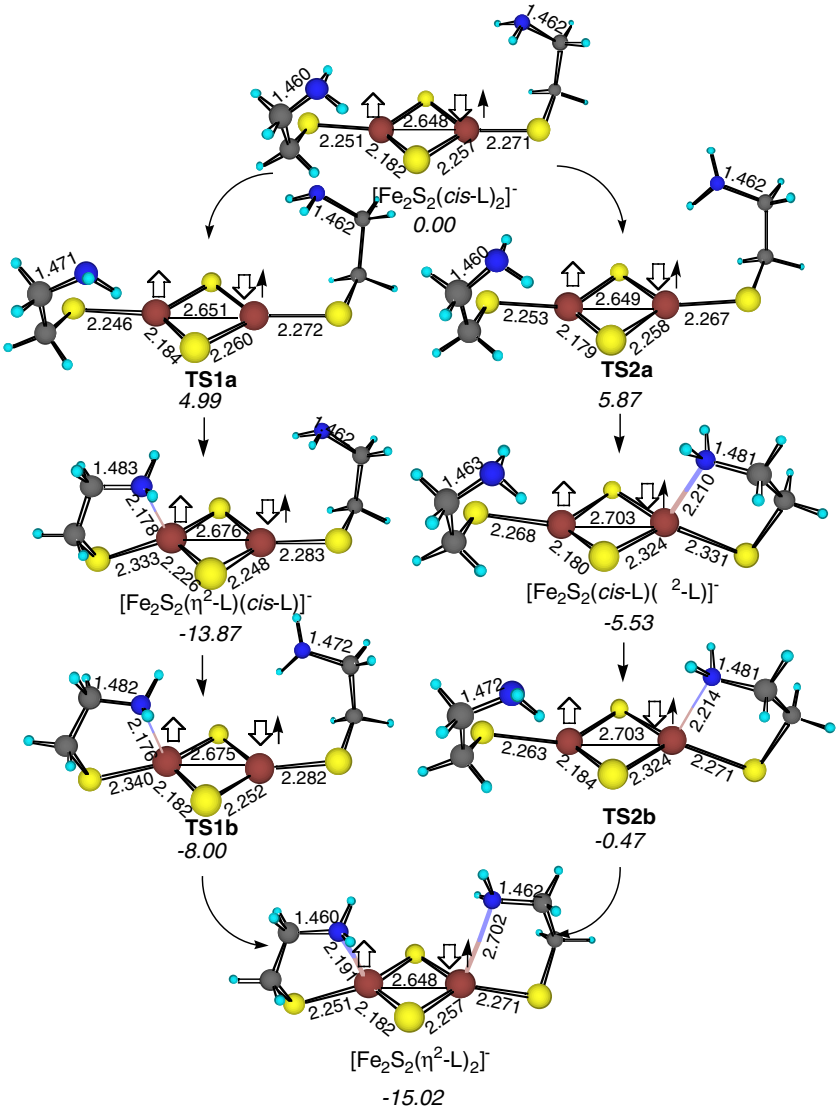


**Fig. 3** The B3LYP/6-31G** optimized geometries and the relative energies (kcal/mol) via the proposed ligand rearrangement of $[Fe_2S_2L_2]^{-}$. The *large hollow arrow* represents the five majority spins, whereas the *small arrow* represents a minority spin on the iron center

observed [2Fe–2S] products. We note that the intensity ratio for the peaks X and X′ (∼0.11) in photoelectron spectroscopy experiment suggested that ∼10% of the fission product was isomer $[Fe_2S_2(\eta^2{-}L)_2]^{-}$ and ∼90% was isomer $[Fe_2S_2(\eta^2{-}L)(cis{-}L)]^{-}$ [16]. Although $[Fe_2S_2(\eta^2{-}L)_2]^{-}$ is the lowest energy isomer, the photoelectron spectroscopy indicates that it is not the predominant species, which suggests that it may be the result of rearrangement of the ligands of $[Fe_2S_2L_2]^{-}$. Overall, it appears that the ligand of $[Fe_2S_2L_2]^{-}$ favors a chelating coordination with the iron center, especially a ferric center, of the [2Fe–2S] cluster in contrast to that in the [4Fe–4S] clusters.

### 3.3 Ligand rearrangement of $[Fe_2S_2(L)_2]^{-}$ (L = –$SC_2H_4NH_2$)

Although $[Fe_2S_2(cis{-}L)_2]^{-}$ and $[Fe_2S_2(cis{-}L)(\eta^2{-}L)]^{-}$ do not appear as final products experimentally, it is possible that they may play a role as intermediates whose ligands rearrange to generate the final observed products. Here, the possible ligand rearrangement processes are examined, specifically, the ligand rearrangement of $[Fe_2S_2(cis-L)_2]^{-}$ through either $[Fe_2S_2(\eta^2-L)(cis-L)]^{-}$ or $[Fe_2S_2(cis-L)(\eta^2-L)]^{-}$ to $[Fe_2S_2(\eta^2-L)_2]^{-}$.

The TS search reveals that the orientation of the $NH_2$ group plays an important role in the ligand rearrangement of $[Fe_2S_2L_2]^{-}$. The DFT TS calculations suggest that the ligand rearrangement from $[Fe_2S_2(cis-L)_2]^{-}$ to $[Fe_2S_2(\eta^2-L)_2]-$ or directly from $[Fe_2S_2(\eta^2-L)(cis-L)]^{-}$ to $[Fe_2S_2(\eta^2-L)_2]^{-}$ primarily involve the rotation of the $NH_2$ group relative to the N–C bond. Overall, the larger exothermicity of −13.87 kcal/mol of the first chelating step and the lower barriers of 5.0 and 5.9 kcal/mol along that reaction route on the left side of Fig. 3 indicate that the reaction pathway from $[Fe_2S_2(cis-L)_2]^{-}$ through **TS1a** to

$[Fe_2S_2(\eta^2-L)(cis-L)]^-$ followed by **TS1b** to $[Fe_2S_2(\eta^2-L)_2]^-$ is not only thermodynamically but also kinetically more favorable over the one through $[Fe_2S_2(cis-L)(\eta^2-L)]^-$ (Fig. 3). Our DFT results suggest that the ligand rearrangement from $[Fe_2S_2(\eta^2-L)(cis-L)]^-$ to $[Fe_2S_2(\eta^2-L)_2]^-$ is slightly exothermic by 1.2 kcal/mol with a barrier of 5.9 kcal/mol. Thus, this observation apparently indicated that the rearrangement of $[Fe_2S_2(\eta^2-L)(cis-L)]^-$ to $[Fe_2S_2(\eta^2-L)_2]^-$ was kinetically controlled (Fig. 3).

Overall, we suggest that the fission of $[Fe_4S_4L_4]^{2-}$ gives $[Fe_2S_2(\eta^2-L)(cis-L)]^-$, which may subsequently rearrange to $[Fe_2S_2(\eta^2-L)_2]^-$. Although we have not yet investigated the direct kinetic processes of the fission to each possible product, $[Fe_2S_2(\eta^2-L)(cis-L)]^-$ is the most likely direct fission product as it is the predominantly observed product experimentally and the barrier for the rearrangement of $[Fe_2S_2(cis-L)_2]^-$ to $[Fe_2S_2(\eta^2-L)(cis-L)]^-$ is large enough so that some $[Fe_2S_2(cis-L)_2]^-$ should be observed if it is a significant direct fission product. Moreover, our proposed mechanism for fission of the spin-delocalized $[Fe_4S_4Cl_4]^{2-}$ involves spin-localization to ferric and ferrous centers, so bidentate coordination of the ferric center may lead to a reduced fission barrier of $[Fe_4S_4L_4]^{2-}$ and a stable $[Fe_2S_2(\eta^2-L)(cis-L)]^-$. Finally, $[Fe_2S_2(\eta^2-L)_2]^-$ most likely occurs via rearrangement of $[Fe_2S_2(\eta^2-L)(cis-L)]^-$ as it is the minor species observed experimentally despite its overall greater stability.

## 4 Conclusion

Combined with recent experimental finding by CID and photoelectron spectroscopy measurements, the structures, energies, and reaction processes for the symmetric fission of $[Fe_4S_4L4]^{2-}$ and the ligand rearrangement of $[Fe_2S_2L_2]^-$ ($L = -SC_2H_4NH_2$) have been investigated by DFT calculations. The $-SC_2H_4NH_2$ ligand in $[Fe_4S_4L_4]^{2-}$ appears to act as a monodentate ligand. In conjunction with the experimental findings, the calculations suggested that $[Fe_2S_2(\eta^2-L)(cis-L)]^-$ and $[Fe_2S_2(\eta^2-L)_2]^-$ are the experimentally observed [2Fe–2S] products and that $[Fe_2S_2(\eta^2-L)_2]^-$ is the result of a kinetically controlled rearrangement of $[Fe_2S_2(\eta^2-L)(cis-L)]^-$.

Overall, the photoelectron spectroscopy and DFT studies reveal critical structural effects on the intrinsic energy and redox properties of iron–sulfur protein analogs. First, the strong bonding interaction between the ferric center and the bidentate ligand contributes to the stability of [2Fe–2S] clusters because $Fe^{III}$ prefers tetra-coordination. The ligand rearrangement of $Fe^{III}$ from the mono- to bidentate coordination leads to an increase of ~0.5 eV in the stabilizing energy and the oxidation energy of $[Fe_2S_2L_2]^-$. Second, although the ligand rearrangement of the ferrous center of $[Fe_2S_2L_2]^-$ from the mono- to bidentate coordination leads to only a slight change of ~0.2 eV in the stabilizing energy, the oxidation energy significantly decreases by ~0.8 eV with the formation of the tetra-coordinated $Fe^{II}$ center. The major factor contributing to this change in the oxidation energy is that the ligand rearrangement of the oxidized iron center dramatically stabilizes the oxidized state, which increases the reducing capability of the $[2Fe–2S]^+$ clusters.

**Acknowledgements** We thank Prof. Lai-Sheng Wang and Dr. You-Jun Fu for the detailed experimental data and valuable discussions. This work was supported by the National Institutes of Health (GM-45303). The calculations were performed at the EMSL, a national user facility sponsored by the US DOE's Office of Biological and Environmental Research located at Pacific Northwest National Laboratory, operated for DOE by Battelle, under the grant GC3565.

## References

1. Beinert H, Holm RH, Munck E (1997) Science 277:653
2. Palmer G (1973) Current insight into the active center of spinach ferredoxin and other iron–sulfur proteins. In: Lovenberg W (ed) iron–sulfur protein Academic, vol II. New York, 285
3. Spiro TG, (ed) (1982) Iron–sulfur proteins, vol IV. Wiley-Interscience, New York
4. Cammack R (1992) Adv Inorg Chem 38:281
5. Beinert H (2000) J Biol Inorg Chem 5:2
6. Wang LS (2001) Clusters. In: Moore JH, Spencer ND (eds) Encyclopedia of chemical physics and physical chemistry, vol III. IOP Publishing, Philadelphia, Vol. III, pp 2113
7. Bertini I, Ciurli S, Luchinat C (1995) The electronic structure of FeS centers in proteins and models: a contribution to the understanding of their electron transfer properties. In: Clarke MJ, Goodenough JB, Jørgensen CK, Mingos DMP, Neilands JB, Palmer GA, Sadler PJ, Weiss R (eds) structure and bonding, vol 83. Springer, Berlin Heidelberg New York, p 1
8. Link TA (1999) Adv Inorg Chem 47:83
9. Leggate EJ, Hirst J (2005) Biochemistry 44:7048
10. Rose K, Shadle SE, Glaser T, de Vries S, Cherepanov A, Canters GW, Hedman B, Hodgson KO, Solomon EI (1999) J Am Chem Soc 121:2353
11. Ullmann GM, Noodleman L, Case DA (2002) J Biol Inorg Chem 7:632
12. Ullmann GM, Noodleman L, Case DA (2001) J Inorg Biochem 86:464
13. Klingen AR, Ullmann GM (2004) Biochemistry 43:12383
14. Yang X, Wang XB, Niu S, Pickett CJ, Ichiye T, Wang LS (2002) Phys Rev Lett 89:163401
15. Niu SQ, Wang XB, Yang X, Wang LS, Ichiye T (2004) J Phys Chem A 108:6750
16. Fu YJ, Niu S, Ichiye T, Wang LS (2005) Inorg Chem 44:1202
17. Mouesca JM, Lamotte B (1998) Coord Chem Rev 180:1573
18. Levine IN (2000) Quantum chemistry, 5th edn Prentice Hall, Upper Saddle River
19. Parr RG, Yang W (1989) Density-functional theory of atoms and molecules. Oxford University Press, Oxford
20. Becke AD (1988) Phys Rev A38:3098
21. Becke AD (1993) J Chem Phys 98:1372
22. Becke AD (1993) J Chem Phys 98:5648
23. Lee C, Yang W, Parr RG (1988) Phys Rev B37:785
24. Rassolov V, Pople JA, Ratner M, Windus TL (1998) J Chem Phys 109:1223
25. Francl MM, Petro WJ, Hehre WJ, Binkley JS, Gordon MS, DeFrees DJ, Pople JA (1982) J Chem Phys 77:3654
26. Hariharan PC, Pople JA (1973) Theor Chim Acta 28:213
27. Simons J, Joergensen P, Taylor H, Ozment J (1983) J Phys Chem 87:2745
28. Banerjee A, Adams N, Simons J, Shepard R (1985) J Phys Chem-Us 89:52
29. Noodleman L, Peng CY, Case DA, Mouesca JM (1995) Coord Chem Rev 144:199

30. Noodleman L (1981) J Chem Phys 74: 5737
31. Wang XB, Niu SQ, Yang X, Ibrahim SK, Pickett CJ, Ichiye T, Wang LS (2003) J Am Chem Soc 125:14072
32. Wang XB, Wang LS (2000) J Chem Phys 112:6959
33. Niu SQ, Wang XB, Nichols JA, Wang LS, Ichiye T (2003) J Phys Chem A 107:2898
34. Niu S, Nichols JA, Ichiye T (in preparation)
35. Yang X, Wang XB, Wang LS, Niu SQ, Ichiye T (2003) J Chem Phys 119:8311
36. Straatsma TP, Aprà E, Windus TL, Bylaska EJ, de Jong W, Hirata S, Valiev M, Hackler M, Pollack L, Harrison R, Dupuis M, Smith DMA, Nieplocha J, Tipparaju V, Krishnan M, Auer AA, Brown E, Cisneros G, Fann G, Früchtl H, Garza J, Hirao K, Kendall R, Nichols J, Tsemekhman K, Wolinski K, Anchell J, Bernholdt D, Borowski P, Clark T, Clerc D, Dachsel H, Deegan M, Dyall K, Elwood D, Glendening E, Gutowski M, Hess A, Jaffe J, Johnson B, Ju J, Kobayashi R, Kutteh R, Lin Z, Littlefield R, Long X, Meng B, Nakajima T, Niu S, Rosing M, Sandrone G, Stave M, Taylor H, Thomas G, van Lenthe J, Wong A, Zhang Z (2004) NWChem, a computational chemistry package for parallel computers, version 4.6. Pacific Northwest National Laboratory, Richland
37. Kendall RA, Apra E, Bernholdt DE, Bylaska EJ, Dupuis M, Fann GI, Harrison RJ, Ju JL, Nichols JA, Nieplocha J, Straatsma TP, Windus TL, Wong AT (2000) Comput Phys Commun 128:260
38. Black G, Didier B, Elsethagen T, Feller D, Gracio D, Hackler M, Havre S, Jones D, Jurrus E, Keller T, Lansing C, Matsumoto S, Palmer B, Peterson M, Schuchardt K, Stephan E, Taylor H, Thomas G, Vorpagel E, Windus T, Winters C (2004) Ecce, a problem solving environment for computational chemistry, software version 3.2.1. Pacific Northwest National Laboratory, Richland